Coherent flow states in a square duct

Håkan Wedin,[1,a)] Damien Biau,[1,b)] Alessandro Bottaro,[1] and Masato Nagata[2]
[1]*DICAT, University of Genova, Via Montallegro 1, 16145 Genova, Italy*
[2]*Department of Aeronautics and Astronautics, Graduate School of Engineering, Kyoto University, Kyoto 606-8501, Japan*

(Received 14 November 2007; accepted 28 July 2008; published online 25 September 2008)

The flow in a square duct is considered. Finite amplitude approximate traveling wave solutions, obtained using the self-sustaining-process approach introduced by Waleffe [Phys. Fluids **9**, 883 (1997)], are obtained at low to moderate Reynolds numbers and used as initial conditions in direct numerical simulations. The ensuing dynamics is analyzed in a suitably defined phase space. Only one among the traveling wave solutions found is capable of surviving for a long time, with the flow trajectory forming quasiregular loops in phase space. Eventually, also this trajectory escapes along the manifold of a chaotic saddle and relaminarization ensues. © *2008 American Institute of Physics*. [DOI: 10.1063/1.2978357]

I. INTRODUCTION

The transition from laminar flow to turbulence in canonical shear flows is still an unsolved matter in fluid mechanics and has for this reason attracted much research interest since the pioneering experimental work by Reynolds[1] in 1883 on pipe flow. Turbulence, albeit chaotic in nature, has a degree of regularity which makes it susceptible to analytical progress as long as irregular flow behavior at small space/time scales does not hide the organized patterns that emerge at larger scales. Current understanding is that whereas small scales of turbulent wall-bounded flows are universal and (almost) autonomous, the larger scales are organized mostly by a linear interaction process with the mean shear. Such a process has been modeled, for example, by rapid distortion theory (RDT), which consists of the solution of the same initial value problem arising in small-perturbation stability analysis, for which only neutral eigenfunctions are available. RDT results in long streaks[2] and this provides a connection to the so-called self-sustaining process (SSP) described by Waleffe[3] to identify large-scale coherent structures in wall-bounded flows.

Before describing recent research on nonlinear, vortical flow solutions, it is appropriate to briefly report on the status of stability and transition in pipe flow. Laminar pipe flow, referred to as Hagen–Poiseuille flow from the independent work of Hagen[4] and Poiseuille,[5] is uniquely realized at low Reynolds numbers $\mathrm{Re}=Ud/\nu$ (U is the streamwise mean velocity, d the pipe diameter, and ν the kinematic viscosity) and has a well known steady parabolic solution. The laminar pipe profile is now believed to be linearly stable for all Re (Refs. 6–10) and numerically proven so for Reynolds numbers up to 10×10^6.[11] Despite this theoretical finding, experiments demonstrate that pipe flow undergoes transition abruptly at moderate Re [$\mathrm{Re}=1750\pm10$ (Refs. 12–14)] where transition is a function of the flow speed, represented by the Reynolds number, plus the form and amplitude of the disturbance. The required disturbance at transition scales as $O(\mathrm{Re}^{-1})$ in the range $1800\leq\mathrm{Re}\leq18000$.[13,15] The same scaling was found theoretically by Gavarini *et al.*[16] Current understanding is that for this flow geometry, transition to turbulence originates from a subcritical instability which triggers perturbations with finite amplitudes that, in turn, bring the flow out of the basin of attraction of the laminar state to a turbulent flow. This scenario might also be at play in the rectangular duct, a case which is linearly stable[17,18] as long as the aspect ratio A of the duct remains below 3.5. By adding an internal heat source, Uhlmann and Nagata[19] found instabilities for $A=1$. Galletti and Bottaro[20] studied the linear nonmodal spatial stability of a square duct flow by imposing secondary structures in the form of optimal streamwise vortices on the basic flow and found the flow to be susceptible to large transient amplifications at finite streamwise lengths before the subsequent viscous decay. The transient growth of disturbance energy and the subsequent formation of streamwise streaks were referred to as likely early stages of transition in a square duct flow. A subsequent attempt to link the algebraic growth to the formation of the large-scale turbulent vortices met with mixed success.[21]

Current wisdom holds that the flow dynamics should be viewed as a time-dependent orbit in phase space among mutually repelling states.[22] Recent evidence[23–28] has shown that chaotic flows (i.e., puff and slugs, see Refs. 29 and 30 for details) may be organized around a more or less large number of equilibrium solutions with large amplitudes (traveling wave solutions) which constitute, in a figurative way of speech, the skeleton of the turbulence. The emergence of the nonlinear traveling wave solutions is now believed to have a strong relation with the observed lower limit of sustainability of turbulence and have been shown to capture the main turbulent statistics.[31,32] Conversely, the numerical simulations by Kerswell and Tutty[33] in a $10R$-long pipe (R is the pipe radius) under turbulent conditions have demonstrated that recurrent traveling wave visits occurred for solutions with low to intermediate wall shear stress for no more than 10%

a)Electronic mail: hakan.wedin@unige.it.
b)Present address: LEA, University of Poitiers, LEA Teleport 2, Bd Marie et Pierre Curie, BP 30179, 86962 Futuroscope Chasseneuil Cedex, France.

of the integration time. The traveling wave solutions are thought to be unstable from the onset[26,33] and are saddle points in phase space to which the flow approaches via the attracting stable manifold; after a few orbits around an unstable (turbulent) node, the flow is ejected in the unstable direction, possibly toward another (unstable) traveling wave solution. The numerical simulation by Faisst and Eckhardt[34] in a pipe with a length of $10R$ showed that the dynamics possesses the properties of a chaotic repellor which switches to a chaotic permanent attractor at $\mathrm{Re}_c=2250$, with lifetime $\tau \propto (\mathrm{Re}_c-\mathrm{Re})^{-1}$. A more recent simulation by Willis and Kerswell[35] found the same distribution with $\mathrm{Re}_c=1870$ in a pipe with a length of $100R$. A corresponding distribution of mean lifetimes was observed in the experiments performed by Peixinho and Mullin,[14] where $\mathrm{Re}_c=1750\pm10$. On the other hand, Hof *et al.*[36] found that τ increases exponentially, implying that turbulence is a decaying event rather than an everlasting occurrence. The review by Eckhardt *et al.*[37] sums up current views on the transition to turbulence in pipe flow; it is believed that many conclusions reported there should apply also to the flow in a square duct.

The fact that the laminar flow in ducts and pipes is linearly stable makes the classical approach for finding nonlinear solutions intractable. Nagata[38] was the first to discover steady nonlinear solutions to a canonical flow (the plane Couette flow) and found three-dimensional (3D) solutions down to Re=125. He circumvented the linear stability issue by starting with the related case of the Taylor–Couette flow between corotating cylinders. The nonlinear solutions were obtained by homotopy, progressively deforming the Taylor–Couette flow until the zero rotation rate case was reached. These results were later refined by Waleffe[31] to Re=127.7 and should be compared to a transitional value of Re =325–360, obtained in laboratory experiments,[39–41] and Re =375 by direct numerical simulations.[42] Six new periodic and relative periodic 3D solutions of turbulent and transitional plane Couette flows have recently been discovered by Viswanath.[43] For the pipe flow Wedin and Kerswell[24] and Faisst and Eckhardt[26] discovered steady nonlinear traveling wave solutions down to Re=1251. To find suitable initial conditions for the nonlinear approach Wedin and Kerswell[24] used the "SSP" procedure initiated by Waleffe.[3] This process employs streamwise rolls, streaks, and traveling waves as a fundamental building block; these structures are capable of generating regions in the flow potentially unstable because of inflectional mechanisms. Recently, Pringle and Kerswell[44] increased the family of traveling wave solutions to pipe flow by discovering solutions down to Re=773 for an azimuthal wavenumber equal to 1. A recent discovery by Wang *et al.*[45] showed that these nonlinear states exist also at very high Reynolds numbers, and thus constitute a robust feature of the dynamics of turbulent flows.

To date, the search for traveling wave solutions in a square duct has not been pursued. Results for this flow case are available from direct numerical simulations and experiments by Gavrilakis,[46] Uhlmann *et al.*,[47] Huser and Biringen,[48] Gessner,[49] and Biau *et al.*,[50] all showing a mean flow with eight vortices in the turbulent regime, with two vortices in each corner, symmetric about the diagonal. This work aims at finding approximate 3D traveling wave solutions to the Navier–Stokes equations in a square duct using the self-sustaining approach mentioned above. These approximate finite amplitude solutions will then serve as initial conditions for direct numerical simulations to assess their robustness and characterize turbulence.

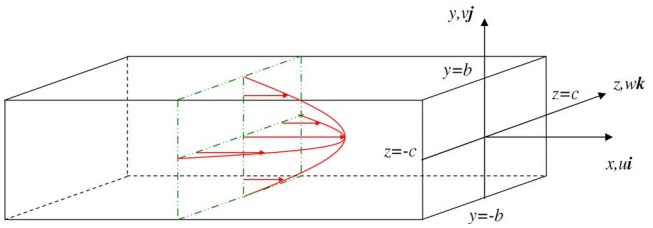

FIG. 1. (Color online) The rectangular duct flow. The flow is confined by the intervals $-\hat{b}\le y\le\hat{b}$ and $-c\le\hat{z}\le\hat{c}$. The unit vectors in the $\hat{x}$, $\hat{y}$, and $\hat{z}$ directions are **i**, **j**, and **k**, respectively. The schematic parabolic-like velocity profile represents the laminar flow.

II. DEFINITIONS AND GOVERNING EQUATIONS

An analysis of an isothermal flow through a rectangular duct under the action of a constant applied pressure gradient in the streamwise direction is performed. The dimensional Cartesian coordinates employed are $\hat{x}$, $\hat{y}$, and $\hat{z}$ and define the streamwise, vertical, and spanwise coordinates, respectively. The corresponding unit vectors are **i**, **j**, and **k** according to Fig. 1, with $\hat{\boldsymbol{u}}=\hat{u}\mathbf{i}+\hat{v}\mathbf{j}+\hat{w}\mathbf{k}$ the velocity vector, $\hat{\rho}$ the fluid density, $\hat{p}$ the pressure, and $\hat{\nu}$ the kinematic viscosity. The flow configuration is defined by the domain $-\hat{b}\le\hat{y}\le\hat{b}$ and $-\hat{c}\le\hat{z}\le\hat{c}$. The aspect ratio A of the duct is defined as $A=\hat{c}/\hat{b}$, where $A=\infty$ corresponds to plane Poiseuille flow and $A=1$ represents a square duct. The dimensional governing equations are the Navier–Stokes and continuity equations

$$\frac{\partial\hat{\boldsymbol{u}}}{\partial\hat{t}}+\hat{\boldsymbol{u}}\cdot\hat{\nabla}\hat{\boldsymbol{u}}=-\frac{1}{\hat{\rho}}\hat{\nabla}\hat{p}+\hat{\nu}\hat{\nabla}^2\hat{\boldsymbol{u}}, \tag{1}$$

$$\hat{\nabla}\cdot\hat{\boldsymbol{u}}=0, \tag{2}$$

with periodic boundary conditions in $\hat{x}$ and no slip at the walls,

$$\hat{\boldsymbol{u}}(\hat{t},\hat{x},\hat{y}=\pm\hat{b},\hat{z})=\hat{\boldsymbol{u}}(\hat{t},\hat{x},\hat{y},\hat{z}=\pm\hat{c})=0. \tag{3}$$

We nondimensionalize the governing equations by using the following scales for length, time, velocity, and pressure:

$$\hat{b},\quad \hat{b}/\bar{\hat{U}}_{\max},\quad \bar{\hat{U}}_{\max},\quad \hat{\rho}\bar{\hat{U}}_{\max}^2. \tag{4}$$

$\bar{\hat{U}}_{\max}$ is the maximum (centerline) laminar streamwise velocity of the flow set in motion by the constant applied pressure gradient $d\bar{\hat{p}}/d\hat{x}$. The overbar defines the mean velocity over the streamwise distance x, i.e.,

$$\bar{u} = \frac{1}{L_x}\int_x u\, dx,$$

where L_x defines the streamwise length of the duct and u represents the streamwise velocity component. The nondimensional bulk velocity is defined as

$$U_b = \frac{1}{4A}\int_{-1}^{+1}\int_{-A}^{+A} \bar{u} dy dz.$$

The Reynolds number Re and the bulk Reynolds number Re_b are defined as

$$\mathrm{Re} = \frac{\hat{\bar{U}}_{\max}\hat{b}}{\hat{\nu}}, \tag{5}$$

$$\mathrm{Re}_b = \frac{\hat{U}_b\hat{b}}{\hat{\nu}}. \tag{6}$$

The nondimensional energy of the mean flow E_U and the fluctuations $E_{u'}$ are defined as

$$E_U = \frac{1}{2}\int_{-1}^{+1}\frac{1}{2A}\int_{-A}^{+A}\frac{1}{2}(\bar{u}^2+\bar{v}^2+\bar{w}^2)dydz,$$

$$E_{u'} = \frac{1}{2}\int_{-1}^{+1}\frac{1}{2A}\int_{-A}^{+A}\frac{1}{2}(u'^2+v'^2+w'^2)dydz,$$

with (u',v',w') fluctuations about the mean. All unknown functions are expanded in the Chebyshev polynomial in the cross section of the duct; hence one needs to map z according to $\eta(z)=z/A$, yielding $-1\le y,\ \eta\le +1$. The nondimensional governing equations are

$$\frac{\partial \boldsymbol{u}}{\partial t} + \boldsymbol{u}\cdot\nabla\boldsymbol{u} = -\nabla p + \frac{1}{\mathrm{Re}}\nabla^2\boldsymbol{u}, \tag{7}$$

$$\nabla\cdot\boldsymbol{u} = 0, \tag{8}$$

with no-slip conditions

$$\boldsymbol{u}(t,x,y=\pm 1,\eta) = \boldsymbol{u}(t,x,y,\eta=\pm 1) = 0. \tag{9}$$

We impose a perturbation $\boldsymbol{u}'=(u',v',w')$ and p' on the laminar flow $\bar{U}(y,\eta)$ and $\bar{p}(x)$. The solution of the flow is thus decomposed into the form

$$\boldsymbol{u}(x,y,\eta,t) = \bar{U}(y,\eta)\mathbf{i} + \boldsymbol{u}'(x,y,\eta,t), \tag{10}$$

$$p(x,y,\eta,t) = \bar{p}_0 + \frac{d\bar{p}}{dx}x + p'(x,y,\eta,t), \tag{11}$$

where $\bar{p}_0$ is an integration constant. The governing equations for the perturbation are thus

$$\frac{\partial \boldsymbol{u}'}{\partial t} + \bar{U}\frac{\partial \boldsymbol{u}'}{\partial x} + \left(v'\frac{\partial \bar{U}}{\partial y} + \frac{1}{A}w'\frac{\partial \bar{U}}{\partial \eta}\right)\mathbf{i} - \frac{1}{\mathrm{Re}}\nabla^2\boldsymbol{u}' + \boldsymbol{u}'\cdot\nabla\boldsymbol{u}' + \nabla p' = 0, \tag{12}$$

$$\nabla\cdot\boldsymbol{u}' = 0. \tag{13}$$

The disturbance is expressed as a traveling wave, i.e.,

$$\boldsymbol{u}' = \sum_{l=-L}^{L}\boldsymbol{u}^{(l)}(y,\eta)e^{Il\alpha(x-ct)}, \tag{14}$$

where $I=\sqrt{-1}$. We represent the unknown functions in the cross section of the duct (y and η) by modified Chebyshev polynomials that are either even or odd and satisfy directly either the homogeneous Dirichlet or the homogeneous Dirichlet and Neumann boundary conditions. The homogeneous Dirichlet and Neumann boundary conditions (denoted by N below) are, starting with the even basis function,

$$\phi_i^N(s) = T_{2i}(s) + (i^2-1)T_0(s) - i^2T_2(s), \quad i=2,3,\ldots,N_s. \tag{15}$$

The odd modified basis is

$$\phi_i^N(s) = T_{2i+1}(s) + \frac{i^2+i-2}{2}T_1(s) - \frac{i^2+i}{2}T_3(s), \quad i=2,3,\ldots,N_s. \tag{16}$$

The even modified basis for the homogeneous Dirichlet boundary conditions (denoted by M below) is

$$\phi_i^M(s) = T_{2i}(s) - T_0(s), \quad i=1,2,3,\ldots,N_s, \tag{17}$$

and the odd modified basis is

$$\phi_i^M(s) = T_{2i+1}(s) - T_1(s), \quad i=1,2,3,\ldots,N_s. \tag{18}$$

The even unconstrained basis function is

$$\phi_i^C(s) = T_{2i}(s), \quad i=0,1,2,3,\ldots,N_s, \tag{19}$$

and the odd basis function is

$$\phi_i^C(s) = T_{2i+1}(s), \quad i=0,1,2,3,\ldots,N_s, \tag{20}$$

where T is the classical Chebyshev polynomial. The collocation grid is defined by the Gauss–Lobatto points

$$s(i) = \cos\left(\frac{i\pi}{N}\right), \quad i=0,1,2,\ldots,N. \tag{21}$$

A. The laminar flow

The steady laminar flow velocity is $\boldsymbol{u}=\bar{U}(y,\eta)\mathbf{i}$, satisfying

$$\frac{\partial^2\bar{U}}{\partial y^2} + \frac{1}{A^2}\frac{\partial^2\bar{U}}{\partial\eta^2} = \mathrm{Re}\frac{d\bar{p}}{dx} \tag{22}$$

with no-slip conditions. The solution for $\bar{U}(y,\eta)$ is expressed in even modified basis functions as

$$\bar{U}(y,\eta) = \sum_{i=1}^{N_y}\sum_{j=1}^{N_z}\hat{U}_{ij}\phi_i^M(y)\phi_j^M(\eta). \tag{23}$$

Since we are using the dimensional laminar centerline velocity $\hat{\bar{U}}_{\max}$ as the characteristic speed, we have $\bar{U}(0,0)=1$.

Hence, we need to apply the particular magnitude of $d\bar{p}/dx$ that produces $\bar{U}(0,0)=1$. The corresponding pressure gradient is $d\bar{p}/dx=-3.393449/\mathrm{Re}$ and the dimensionless bulk velocity is $U_b=0.4770$.

III. THE SELF-SUSTAINING PROCESS

The SSP introduced by Waleffe[3] and applied successfully by Waleffe[31,51] and Wedin and Kerswell[24] is at the heart of the present approach to find approximate solutions (or SSP solutions) to the Navier–Stokes equations. The approximate solutions will subsequently serve as initial conditions in direct numerical simulations. Following the basic concept of Waleffe for the SSP, we decompose the flow components in Eq. (14) into three parts,

$$\begin{bmatrix} \boldsymbol{u}' \\ p' \end{bmatrix} = \begin{bmatrix} 0 \\ \tilde{V}(y,\eta) \\ \tilde{W}(y,\eta) \\ \tilde{P}(y,\eta) \end{bmatrix}_{\text{rolls}} + \begin{bmatrix} \tilde{U}(y,\eta) \\ 0 \\ 0 \\ 0 \end{bmatrix}_{\text{streaks}} + \begin{bmatrix} \hat{u}(x,y,\eta,t) \\ \hat{v}(x,y,\eta,t) \\ \hat{w}(x,y,\eta,t) \\ \hat{p}(x,y,\eta,t) \end{bmatrix}_{\text{waves}}. \tag{24}$$

In short, the main step of the SSP is the exponential instability of a steady velocity field composed by the laminar flow and velocity streaks of $O(1)$ and streamwise rolls with amplitudes $\ll 1$. The eigenfunctions of the instability are 3D and include quasistreamwise vortex pairs of $O(\mathrm{Re}^{-1})$. The flow components in Eq. (24) put together would create a flow behaving in a similar fashion as the wavy unstable streak structures observed in the experiments by Kline *et al.*[52] A neutral instability of the mean flow allows to convert these vortex pairs into two-dimensional rolls. The mean shear has a dual role in this process; it provides energy to the exponential instability of the streaky flow, and it is deformed by the rolls, via the lift-up effect, so that streaks are recreated. The corresponding solutions should in general give good descriptions of the full nonlinear solutions to the Navier–Stokes equations because of the appropriate approximations made in the SSP, i.e., the amplitude of the rolls is set very low and the amplitude of the waves is assumed to be small, therefore justifying the linearization of the equations defining the rolls, the streaks, and the waves. However, previous studies[24] showed that it is not always that the SSP solutions lead directly to nonlinear states. Discovering approximate solutions, using the SSP, gives directions on where to start searching for the nonlinear traveling wave solutions. Former studies[24,26,27] showed the relevance of the traveling waves to the understanding of turbulence.

A. The streamwise rolls

The equations governing the streamwise rolls are obtained by streamwise averaging the cross-flow components of Eq. (12). We represent the streamwise rolls by the stream function $\psi(t,y,\eta)$ according to the following definition:

$$V=\frac{1}{A}\frac{\partial\psi}{\partial\eta}, \tag{25}$$

$$W=-\frac{\partial\psi}{\partial y}, \tag{26}$$

so that continuity is automatically satisfied. By taking $\mathbf{i}\cdot\nabla\times(\,)$ of the streamwise-averaged version of Eq. (12) we arrive at the governing equation for ψ,

$$\frac{\partial}{\partial t}\nabla^2\psi=\frac{1}{\mathrm{Re}}\nabla^4\psi+\mathcal{N}(\psi)+\mathbf{i}\cdot\nabla\times(\overline{\hat{\boldsymbol{u}}\cdot\nabla\hat{\boldsymbol{u}}}). \tag{27}$$

Here $\hat{\boldsymbol{u}}$ corresponds to the waves and $\mathcal{N}(\psi)$ is the nonlinear terms of ψ. To reach a defining equation for the stream function we linearize with respect to ψ and $\hat{\boldsymbol{u}}$ (assuming their amplitudes to be small). Further, by assuming the solution to behave as $\psi=\tilde{\psi}(y,\eta)e^{\lambda t/\mathrm{Re}}$ the following eigenvalue problem is found:

$$\lambda\nabla^2\tilde{\psi}=\nabla^4\tilde{\psi} \tag{28}$$

with boundary conditions

$$\begin{aligned}\tilde{\psi}(y=\pm1,\eta)&=\frac{\partial\tilde{\psi}}{\partial y}(y=\pm1,\eta)\\&=\tilde{\psi}(y,\eta=\pm1)\\&=\frac{\partial\tilde{\psi}}{\partial\eta}(y,\eta=\pm1)=0.\end{aligned} \tag{29}$$

The function $\tilde{\psi}$ is expanded in odd basis functions as

$$\tilde{\psi}(y,\eta)=\sum_{i=2}^{N_y}\sum_{j=2}^{N_z}\hat{\psi}_{ij}\phi_i^N(y)\phi_j^N(\eta). \tag{30}$$

Earlier studies showed that four- and eight-vortex structures are relevant in turbulent flows.[46,47] By imposing the odd symmetry on $\tilde{\psi}(y,\eta)$ the two least stable modes will show the above mentioned vortex structures. In order to set an amplitude, $\tilde{\psi}$ is normalized as

$$\frac{\tilde{\psi}(y,\eta)}{\|\tilde{\psi}(y,\eta)\|_\infty}. \tag{31}$$

The arbitrary phase of $\tilde{\psi}$ is fixed by normalizing the function such that

$$\frac{\partial\tilde{\psi}}{\partial y}(0,0.45)>0. \tag{32}$$

All eigenmodes of Eq. (28) are decaying; see Table I. We will focus on the two least stable modes ($n=1$ and $n=2$) as

TABLE I. The five least stable eigenvalues λ of the symmetric stream function in a square duct.

n	1	2	3	4	5
λ_n	−32.052	−67.280	−69.770	−100.967	−125.255

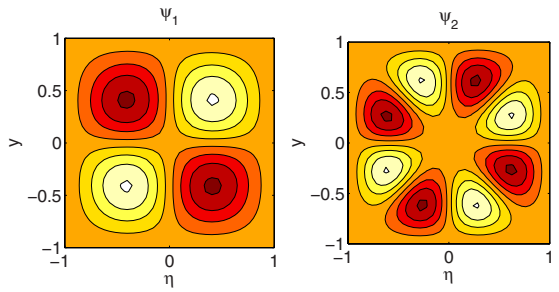

FIG. 2. (Color online) Plot of the two least stable symmetric modes of Eq. (28). The color coding goes from most negative (darkest) to most positive (lightest).

initial structures of the stream function displayed in Fig. 2. Figure 3 shows the streamwise-averaged part of the successful SSP solutions found at Re=3000 and 5000 with an amplitude $\|\tilde{\psi}_n\|=0.002$ and $n=1$ ($\lambda_1=-32.052$).

B. The streamwise streaks

The equation governing the unsteady streaks $U(t,y,\eta)$ is obtained by streamwise averaging the streamwise component of Eq. (12), i.e.,

$$\frac{\partial U}{\partial t}+\frac{1}{A}\frac{\partial\tilde{\psi}}{\partial\eta}\frac{\partial U}{\partial y}-\frac{1}{A}\frac{\partial\tilde{\psi}}{\partial y}\frac{\partial U}{\partial\eta}-\frac{1}{\mathrm{Re}}\nabla^2 U = -\frac{1}{A}\frac{\partial\tilde{\psi}}{\partial\eta}\frac{\partial\bar{U}}{\partial y}+\frac{1}{A}\frac{\partial\tilde{\psi}}{\partial y}\frac{\partial\bar{U}}{\partial\eta}-\overline{\hat{\boldsymbol{u}}\cdot\nabla\hat{\boldsymbol{u}}}. \tag{33}$$

Then, omitting the quadratic term in $\hat{\boldsymbol{u}}$ and considering steady streaks $\tilde{U}(y,\eta)$, we arrive at

$$\frac{1}{A}\frac{\partial\tilde{\psi}}{\partial\eta}\frac{\partial\tilde{U}}{\partial y}-\frac{1}{A}\frac{\partial\tilde{\psi}}{\partial y}\frac{\partial\tilde{U}}{\partial\eta}-\frac{1}{\mathrm{Re}}\nabla^2\tilde{U}=-\frac{1}{A}\frac{\partial\tilde{\psi}}{\partial\eta}\frac{\partial\bar{U}}{\partial y}+\frac{1}{A}\frac{\partial\tilde{\psi}}{\partial y}\frac{\partial\bar{U}}{\partial\eta}. \tag{34}$$

The streaks are even in y and η and are expanded as

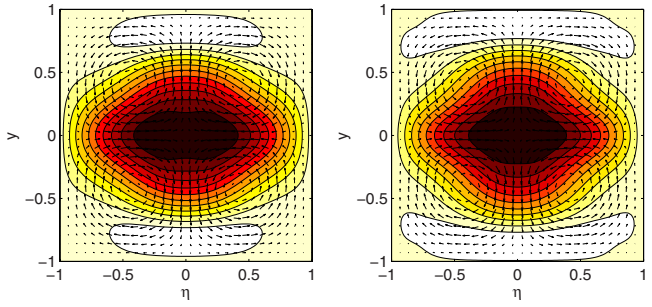

FIG. 3. (Color online) The streamwise rolls (arrows) $[\tilde{V}(y,\eta),\tilde{W}(y,\eta)]$ and streamwise streaks (contour levels) $\tilde{U}(y,\eta)$ at $A=1$, $\|\tilde{\psi}_1\|=0.002$. Left plot: The flow at Re=3000 and the contour levels range between the minimum and the maximum of $\tilde{U}(y,\eta)$ or −0.5263 to 0.0705 in steps of 0.05. Right plot: Re=5000 and the contour levels range between the minimum and the maximum of $\tilde{U}(y,\eta)$ or −0.5953 to 0.0567 in steps of 0.06. The color coding goes from most negative (darkest) to most positive (lightest).

$$\tilde{U}(y,\eta)=\sum_{i=1}^{N_y}\sum_{j=1}^{N_z}\hat{U}_{ij}\phi_i^M(y)\phi_j^M(\eta) \tag{35}$$

with the boundary conditions

$$\tilde{U}(y=\pm 1,\eta)=\tilde{U}(y,\eta=\pm 1)=0. \tag{36}$$

Equation (34) models the action of the stream function (rolls) on the streaks by the lift-up effect.

C. The linear instability analysis

The linear stability of the steady basic flow composed by the laminar profile, the rolls, and the streaks is studied next, and to obtain a nongrowing solution we search for neutrally stable waves. The equations governing the waves ($\hat{u}$, $\hat{v}$, $\hat{w}$, and $\hat{p}$) are obtained by subtracting the equations that define the rolls and the streaks from Eq. (12). Thus we have

$$\frac{\partial\hat{\boldsymbol{u}}}{\partial t}+\tilde{\boldsymbol{U}}\cdot\nabla\hat{\boldsymbol{u}}+\hat{\boldsymbol{u}}\cdot\nabla\tilde{\boldsymbol{U}}+\nabla\hat{p}-\frac{1}{\mathrm{Re}}\nabla^2\hat{\boldsymbol{u}}+\bar{U}\frac{\partial\hat{\boldsymbol{u}}}{\partial x}+\left(\hat{v}\frac{\partial\bar{U}}{\partial y}+\frac{1}{A}\hat{w}\frac{\partial\bar{U}}{\partial\eta}\right)\mathbf{i}=-\hat{\boldsymbol{u}}\cdot\nabla\hat{\boldsymbol{u}}-\begin{bmatrix}0\\ \tilde{\boldsymbol{U}}\cdot\nabla\tilde{V}\\ \tilde{\boldsymbol{U}}\cdot\nabla\tilde{W}\end{bmatrix}, \tag{37}$$

$$\nabla\cdot\hat{\boldsymbol{u}}=0. \tag{38}$$

Neglecting the right-hand side of Eq. (37) (assuming small amplitudes for rolls $\tilde{\boldsymbol{U}}$ and waves $\hat{\boldsymbol{u}}$) yields the governing equations for the linear waves. Since the basic flow is independent of x and t, the solution of Eqs. (37) and (38) can be expressed as

$$\begin{bmatrix}\boldsymbol{u}-\bar{U}\mathbf{i}\\ p-\left(p_0+\frac{d\bar{p}}{dx}x\right)\end{bmatrix}=\begin{bmatrix}\hat{\boldsymbol{u}}\\ \hat{p}\end{bmatrix}=\begin{bmatrix}u(y,\eta)\\ v(y,\eta)\\ w(y,\eta)\\ p(y,\eta)\end{bmatrix}e^{I\alpha(x-ct)}+\text{c.c.}$$
$$=\begin{bmatrix}\sum_{i=1}^{N_y}\sum_{j=1}^{N_z}\tilde{u}_{ij}\phi_i^M(y)\phi_j^M(\eta)\\ \sum_{i=2}^{N_y}\sum_{j=1}^{N_z}\tilde{v}_{ij}\phi_i^N(y)\phi_j^M(\eta)\\ \sum_{i=1}^{N_y}\sum_{j=2}^{N_z}\tilde{w}_{ij}\phi_i^M(y)\phi_j^N(\eta)\\ \sum_{i=0}^{N_y}\sum_{j=0}^{N_z}\tilde{p}_{ij}\phi_i^C(y)\phi_j^C(\eta)\end{bmatrix}e^{I\alpha(x-ct)}+\text{c.c.} \tag{39}$$

c.c. stands for complex conjugate, α is the streamwise wavenumber of the instability, and the eigenvalue c is given by $c=c_r+ic_i$, where αc_i is the growth rate and αc_r is the frequency of the wave. For $\alpha c_i>0$ the solution grows with time. We reduce the system of equations in Eqs. (37) and (38) down to two by eliminating $u(y,\eta)$ and $p(y,\eta)$ by solving for $u(y,\eta)$ in the continuity equation (38) and for $p(y,\eta)$

TABLE II. The four possible symmetries for the linear waves, even (e) and odd (o).

I	$u(o,e)$	$v(e,e)$	$w(o,o)$	$p(o,e)$
II	$u(o,o)$	$v(e,o)$	$w(o,e)$	$p(o,o)$
III	$u(e,e)$	$v(o,e)$	$w(e,o)$	$p(e,e)$
IV	$u(e,o)$	$v(o,o)$	$w(e,e)$	$p(e,o)$

in the u-momentum equation.[17] Next, we substitute $u(y,\eta)$ and $p(y,\eta)$ into the remaining equations, i.e., the v momentum and the w momentum, yielding two governing equations of order 4 for $\hat{v}$ and $\hat{w}$, leading to an $N\times N$ matrix with $N=2N_yN_z-N_y-N_z$. Finally we enforce the y- and η-dependent equations by a Galerkin projection over y and η to form an eigenvalue problem of the form $c\boldsymbol{A}\cdot\tilde{\boldsymbol{u}}=\boldsymbol{B}\cdot\tilde{\boldsymbol{u}}$. The linear governing equations are projected as follows:

$$c\int_{y=-1}^{+1}\int_{\eta=-1}^{+1}\frac{\boldsymbol{C}(y,\eta)\phi_k(y)\phi_l(\eta)}{W(y)W(\eta)}dyd\eta = \int_{y=-1}^{+1}\int_{\eta=-1}^{+1}\frac{\boldsymbol{D}(y,\eta)\phi_k(y)\phi_l(\eta)}{W(y)W(\eta)}dyd\eta, \tag{40}$$

where $\boldsymbol{C}$ corresponds to the time derivative of $\hat{\boldsymbol{u}}$ and $\boldsymbol{D}$ to the remaining terms in the linear stability equations, functions with indices k and l are the test functions, and $W(y)$ and $W(\eta)$ are the weight functions associated with the classical Chebyshev polynomial, i.e.,

$$W(\xi)=\sqrt{1-\xi^2}. \tag{41}$$

The symmetries and the end point conditions of the test functions $\phi_k(y)$ and $\phi_l(\eta)$ vary as a function of the governing equation in question. In this circumstance the test functions in the v momentum equals the expansions in y and η for $v(y,\eta)$; for the w momentum the test functions equal the expansions for $w(y,\eta)$. The boundary conditions for the perturbations are

$$\hat{\boldsymbol{u}}(t,x,y=\pm 1,\eta)=\hat{\boldsymbol{u}}(t,x,y,\eta=\pm 1)=0, \tag{42}$$

$$\frac{\partial\hat{v}}{\partial y}(t,x,y=\pm 1,\eta)=\frac{\partial\hat{w}}{\partial\eta}(t,x,y,\eta=\pm 1)=0, \tag{43}$$

where $\hat{\boldsymbol{u}}=(\hat{u},\hat{v},\hat{w})$. To compute the integral in Eq. (40) the basis functions for all derivatives involved are converted into a sum of Chebyshev polynomials. Doing this, the orthogonality of the Chebyshev polynomials can be benefited from and the integrals can be computed exactly. The four possible symmetries admitted by the linearized Navier–Stokes equations and the continuity equation are those of Table II and are the same symmetries as in Ref. 17. We will put focus on symmetry I since it is reported to be the least stable one according to Tatsumi and Yoshimura[17] even though this is not necessarily the case in general. Symmetry I in turn defines the symmetries for the stream function $\tilde{\psi}(y,\eta)$ and the streaks $\tilde{U}(y,\eta)$. A successful comparison has been made with the linear stability analysis of the laminar flow performed by Tatsumi and Yoshimura[17] and Theofilis *et al.*[18] The stability of the basic flow field represented by the laminar flow, the stream function, plus the streaks has been confirmed by an independent code to perfect agreement. The linear stability analysis extends over the following intervals: Re $\in[3000,5000,7000]$, $0\leq\alpha\simeq 11$, for the amplitude of the stream function $\|\tilde{\psi}_n\|=0.002$. The chosen eigenmodes of the stream function $\tilde{\psi}_n$ are $n=1$ and $n=2$. The value Re=3000 is close to the limit where marginal turbulence is observed. A truncation of $(N_y,N_z)=(20,20)$ proved to be sufficient for the $n=1$ case except at high α for Re=7000, where a convergence of the eigenvalue and eigenfunction at neutral stability was obtained by using $(N_y,N_z)=(30,30)$. For the $n=2$ case a (30,30) truncation is required over the parameters studied. The search for the neutrally stable modes was terminated when $|c_i|<1\times10^{-5}$. Figure 4 shows the most unstable mode at Re=3000, $A=1$, $\|\tilde{\psi}_1\|=0.002$ for symmetry I and the two waves (encircled at $\alpha=0.282$ and $\alpha=1.5$), leading to a "good" SSP solution (as will be justified in Sec. III D). Figure 5 at Re=5000 shows the mode contributing to a good SSP solution at $\alpha=3.415$ (encircled). At this particular wavenumber there is also an unstable mode (shown in the figure with diamond-shaped symbols). We discard this mode since we are looking for steady SSP solutions, i.e., neutrally stable waves that do not amplify in time. The two neutral points ($\alpha\approx 2.3$ and $\alpha\approx 4.5$) on this mode lead to unacceptable SSP solutions, suggesting that this particular mode is not pertinent in a self-sustaining sense. All three neutral waves move at approximately the speed of the laminar bulk flow. Figures 6–8 show the eigenfunctions of the waves at the parameter values that provide good feedback for the SSP process. In these three figures the phase of the solution is fixed by forcing $\mathrm{Im}[v(0.5,0.5)]=0$.

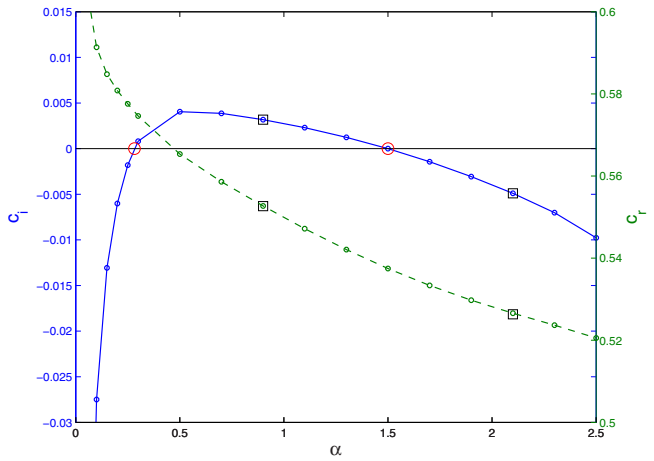

FIG. 4. (Color online) The growth rate c_i (solid line) and the phase speed c_r (dashed line) as a function of the streamwise wavenumber α at Re=3000, $A=1$, $\|\tilde{\psi}_1\|=0.002$, and symmetry I of the wave. The points of neutral stability ($c_i=0$) are indicated by the two bigger circles and serve as the wavy part of the SSP. The squares are obtained with $(Ny,Nz)=(30,30)$ and confirm that a resolution with $(Ny,Nz)=(20,20)$ is adequate.

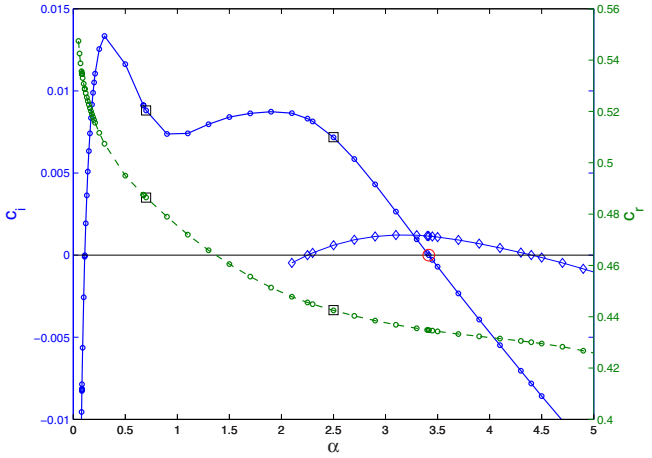

FIG. 5. (Color online) The growth rate c_i (solid line) and the phase speed c_r (dashed line) as a function of the streamwise wavenumber α at Re=5000, $A=1$, $\|\tilde{\psi}_1\|=0.002$, and symmetry I of the wave. The point of neutral stability ($c_i=0$) is pointed out by the bigger circle and serves as the wavy part of the SSP solution. The squares are solutions with $(Ny,Nz)=(30,30)$. The curve marked by ◇ shows the unstable mode at $\alpha=3.415$.

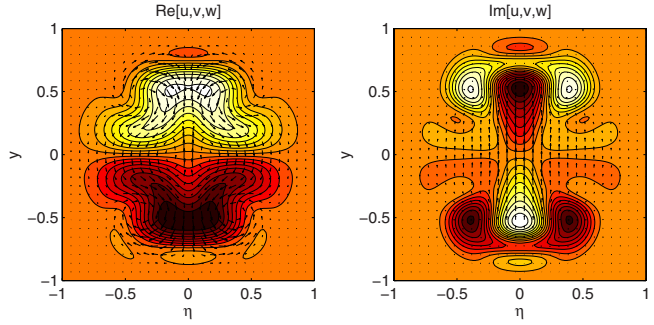

FIG. 7. (Color online) The real and the imaginary part of the eigenfunction of the wave at Re=3000, $A=1$, $\alpha=1.5$, $\|\tilde{\psi}_1\|=0.002$, and symmetry I of the wave. This solution corresponds to the point of neutral stability in Fig. 4. The arrows correspond to the cross-section velocity of the wave $[0,v,w]$. Left plot: The contour levels range between the minimum and the maximum of Re$[u]$ or −0.0138 to 0.0138 in steps of 0.0017. Right plot: The contour levels range between the minimum and the maximum of Im$[u]$ or −0.0054 to 0.0054 in steps of 0.00065. The color coding goes from most negative (darkest) to most positive (lightest).

D. The feedback

The steady equation governing the feedback of the initial stream function is obtained by accounting for the nonlinear interaction of the waves on the rolls in Eq. (27), thus producing re-energized rolls noted $\tilde{\psi}^r$. Linearizing with respect to $\tilde{\psi}^r$ yields

$$\frac{1}{\mathrm{Re}}\nabla^4\tilde{\psi}^r(y,\eta) = -\mathbf{i}\cdot\nabla\times(\overline{\hat{\boldsymbol{u}}\cdot\nabla\hat{\boldsymbol{u}}}). \tag{44}$$

In order to obtain an acceptable approximate solution to the Navier–Stokes equations we need to make sure that the forced or re-energized $\tilde{\psi}^r(y,\eta)$ is close to the initial $\tilde{\psi}$ found from Eq. (28). Since the initial stream function, used both in the equation for the streaks and in the linear wave equations, has a set amplitude, we multiply $\psi^r(y,\eta)$ by the set amplitude $\|\tilde{\psi}_n\|$ in Eq. (44) and adjust the unknown wave amplitude ϵ so that $\max[\tilde{\psi}^r(y,\eta)]=1$. An approximate solution, consisting of the stream function (rolls), streaks, and waves, to the Navier–Stokes equations is obtained upon finding a good match between the re-energized $\tilde{\psi}^r$ and the initial stream function $\tilde{\psi}$. The solutions are parametrized by the Re, α, and A.

Figure 9 shows the feedback for the first bifurcation point at $\alpha=0.282$ and Re=3000 (see encircled point with $c_i=0$ in Fig. 4) for six values of η, where η is indicated at the top of each subplot. We observe good match overall, with better agreement near the walls. Good match is the hallmark of efficient feedback, although this still has to be verified independently. Figure 10 shows also a good feedback using the solution of the linear waves $\alpha=1.5$ (see encircled point with $c_i=0$ in Fig. 4). Similarly (not shown), we obtain another good SSP solution for Re=5000, $\alpha=3.415$.

Over the parameter space covered no SSP solutions were found for the $\tilde{\psi}_2$ eigenmode of the initial stream function

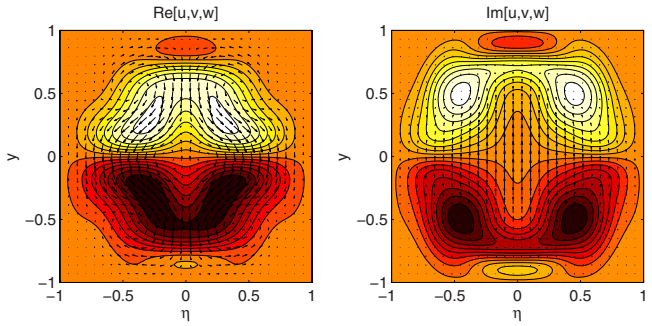

FIG. 6. (Color online) The real and the imaginary part of the eigenfunction of the wave at Re=3000, $A=1$, $\alpha=0.282$, $\|\tilde{\psi}_1\|=0.002$, and symmetry I of the wave. This solution corresponds to the point of neutral stability ($c_i=0$) in Fig. 4. The arrows correspond to the cross-section velocity of the wave or $v(y,\eta)$ and $w(y,\eta)$. Left plot: The contour levels range between the minimum and the maximum of Re$[u(y,\eta)]$ or −0.0649 to 0.0649 in steps of 0.009. Right plot: The contour levels range between the minimum and the maximum of Im$[u(y,\eta)]$ or −0.0246 to 0.0246 in steps of 0.003. The color coding goes from most negative (darkest) to most positive (lightest).

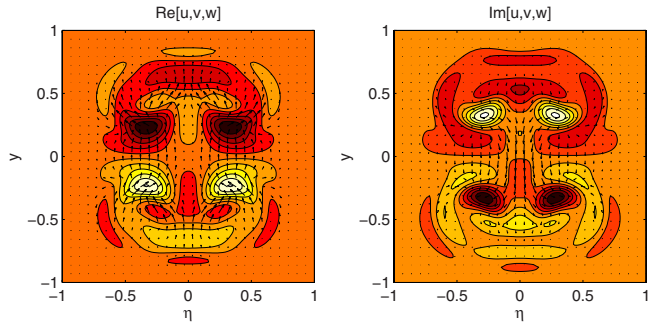

FIG. 8. (Color online) The real and the imaginary parts of the eigenfunction of the wave at Re=5000, $A=1$, $\alpha=3.415$, $\|\tilde{\psi}_1\|=0.002$, and symmetry I of the wave. This solution corresponds to the point of neutral stability in Fig. 5. The arrows correspond to the cross-section velocity of the wave $[0,v,w]$. Left plot: The contour levels range between the minimum and the maximum of Re$[u]$ or −0.011 to 0.011 in steps of 0.002. Right plot: The contour levels range between the minimum and the maximum of Im$[u]$ or −0.0077 to 0.0077 in steps of 0.0015. The color coding goes from most negative (darkest) to most positive (lightest).

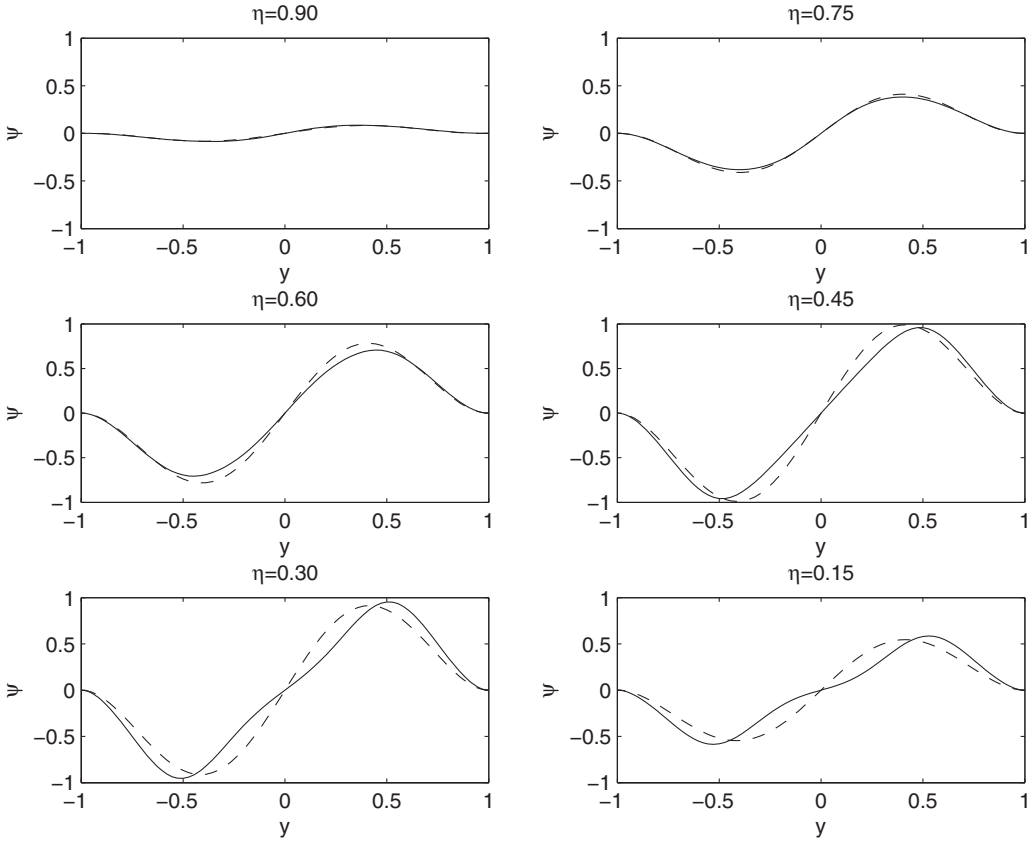

FIG. 9. The feedback of the stream function at six stations in η at Re=3000, $A=1$, $\|\tilde{\psi}_1\|=0.002$, $\alpha=0.282$, and symmetry I of the wave. The dashed line corresponds to the initial stream function $\bar{\psi}(y,\eta)$ and the solid line to the $\bar{\psi}'(y,\eta)$. The value of η is indicated at the top of each individual figure.

(corresponding to eight vortices, two in each corner). Although this might seem disappointing at first sight, given the known features of coherent structures in a square duct,[46] recent evidence[47] shows that the eight-vortex pattern results from the superposition of four-vortex states provided that sufficiently long averaging periods are considered. Table III shows the properties of the SSP solutions found.

IV. DIRECT NUMERICAL SIMULATIONS

Temporally evolving simulations have been conducted in a periodic duct with streamwise length L_x using the solutions obtained in Sec. III as initial conditions. For each direct numerical simulation the initial state consists of the ideal base flow profile $\bar{U}(y,\eta)$ plus the approximation of an "exact coherent state" plus random noise. The very low complex amplitude of the noise in Fourier space varies between $\pm 10^{-10}$; the noise is necessary to fill the spectrum. The parameters used for the three cases studied are summarized in Table IV. In all cases we have opted to use a computational domain as long as possible; in the case $\alpha_{\mathrm{TW}}=0.282$, only one period of oscillations could be accommodated to maintain a reasonable computational cost.

A. Definitions

By normalizing variables with the half channel height $\hat{b}$, the centerline velocity $\bar{\hat{U}}_{\max}$, time with $\hat{b}/\bar{\hat{U}}_{\max}$, and pressure with $\hat{\rho}\bar{\hat{U}}_{\max}^2$, we arrive at the nondimensional Navier–Stokes equations

$$\frac{\partial u}{\partial x}+\frac{\partial v}{\partial y}+\frac{1}{A}\frac{\partial w}{\partial \eta}=0, \tag{45}$$

$$\frac{\partial u}{\partial t}+u\frac{\partial u}{\partial x}+v\frac{\partial u}{\partial y}+\frac{w}{A}\frac{\partial u}{\partial \eta}=-\frac{\partial p}{\partial x}+\frac{1}{\mathrm{Re}}\nabla^2 u-\frac{d\bar{p}}{dx}, \tag{46}$$

$$\frac{\partial v}{\partial t}+u\frac{\partial v}{\partial x}+v\frac{\partial v}{\partial y}+\frac{w}{A}\frac{\partial v}{\partial \eta}=-\frac{\partial p}{\partial y}+\frac{1}{\mathrm{Re}}\nabla^2 v, \tag{47}$$

$$\frac{\partial w}{\partial t}+u\frac{\partial w}{\partial x}+v\frac{\partial w}{\partial y}+\frac{w}{A}\frac{\partial w}{\partial \eta}=-\frac{1}{A}\frac{\partial p}{\partial \eta}+\frac{1}{\mathrm{Re}}\nabla^2 w, \tag{48}$$

with $\mathrm{Re}=\bar{\hat{U}}_{\max}\hat{b}/\hat{\nu}$. We fix the pressure gradient in the duct to $\bar{p}_x=-3.393449/\mathrm{Re}$; this value corresponds to a centerline velocity equal to 1 in the laminar case. The skin friction is defined as $f=8\hat{u}_\tau^2/\hat{U}_b^2$, where $\hat{u}_\tau^2=(-2\hat{b}/4\hat{\rho})\bar{\hat{p}}_x$. In the streamwise direction the flow field is expanded in Fourier basis as

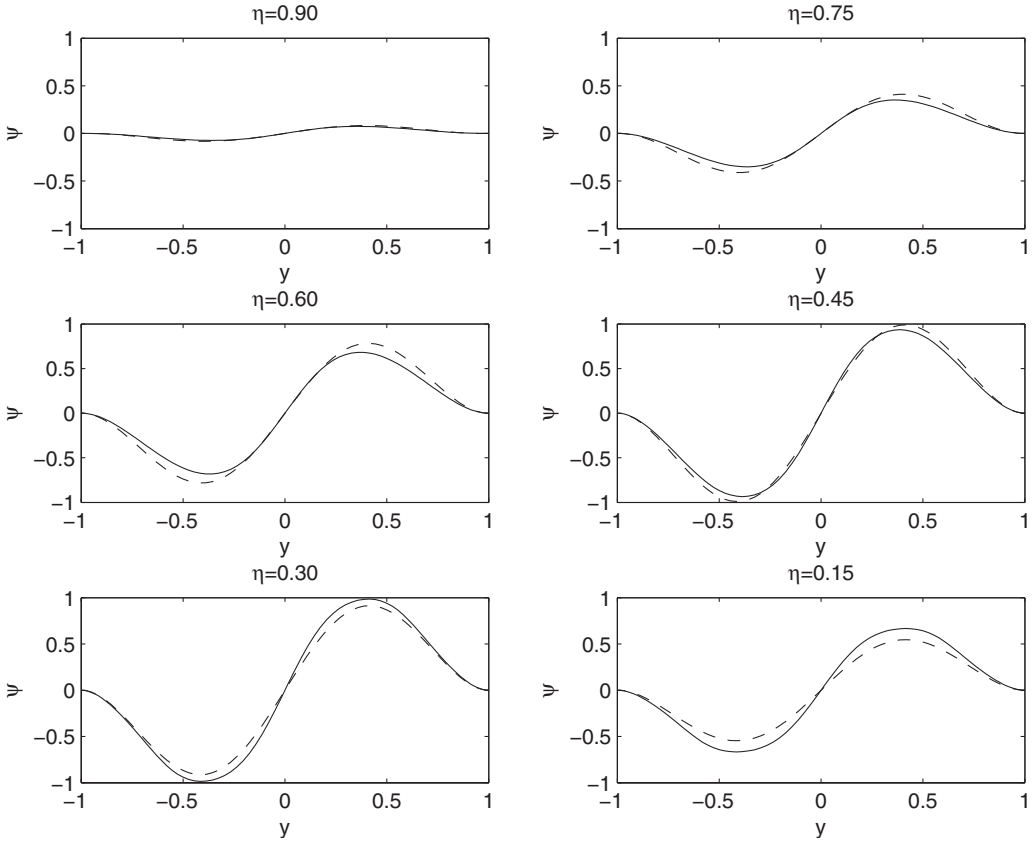

FIG. 10. The feedback of the stream function at six stations in η at Re=3000, $A=1$, $\|\tilde{\psi}_1\|=0.002$, $\alpha=1.5$, and symmetry I of the wave. The dashed line corresponds to the initial stream function $\tilde{\psi}(y,\eta)$ and the solid line to the $\tilde{\psi}'(y,\eta)$. The value of η is indicated at the top of each individual figure.

$$\boldsymbol{u}(t,x,y,\eta)=\sum_{n=-N}^{N}\hat{\boldsymbol{u}}_n(t,y,\eta)e^{I\alpha_n x}. \tag{49}$$

The mean flow is represented by the $n=0$ mode and consists of the ideal laminar flow, the streaks, and the rolls. The fluctuations correspond to the modes with $n\neq 0$. An incompressible Navier–Stokes spectral numerical solver, based on Chebyshev collocation in y and η and Fourier transform along x, has been employed to solve these equations.[50] Numerical tests have shown that a sufficient number of cross-stream Chebyshev points proved to be 36×36, with $N_x=64$ streamwise grid points or 41 Fourier modes after dealiasing. For all cases the time step is constant: $\Delta t=10^{-2}$. This numerical method provides an excellent match with the turbulent results by Gavrilakis[46] at the same Re.

B. Results

In Fig. 11 the time evolution of the energy of the fluctuations is plotted for short times. The initial condition is the SSP solutions at $\alpha_{\mathrm{TW}}=0.282$ (dashed line), $\alpha_{\mathrm{TW}}=1.5$ (solid line), and $\alpha_{\mathrm{TW}}=3.415$ (dash-dotted line). After approximately 500 time units the energy of the fluctuations essentially vanishes for the cases of $\alpha_{\mathrm{TW}}=0.282$ and $\alpha_{\mathrm{TW}}=3.415$ whereas for the case $\alpha_{\mathrm{TW}}=1.5$ the fluctuations are still finite and slowly increasing in magnitude. In agreement with the numerically computed SSP solutions (see Sec. III) we observe both for $\alpha_{\mathrm{TW}}=1.5$ and $\alpha_{\mathrm{TW}}=3.415$ a self-sustained solution up to approximately 150 time units, whereas for $\alpha_{\mathrm{TW}}=0.282$ there is a monotonic decay in the disturbance energy. In the remaining part of this work we will devote attention to the $\alpha_{\mathrm{TW}}=1.5$ case since this was the only case that proved to sustain a large amplitude vortical state for long

TABLE III. Properties of the discovered SSP solutions. The measure of the amplitude of the rolls is defined as $\tilde{\boldsymbol{U}}_\perp=\tilde{V}\boldsymbol{j}+\tilde{W}\boldsymbol{k}$.

Re	α	$\|\tilde{\psi}_1\|$	$\|\tilde{\boldsymbol{U}}_\perp\|$	$\|\hat{\boldsymbol{U}}\|$	c_r	c_i (10^{-6})
3000	0.282	0.002	0.0077	0.526	0.576	2.63
3000	1.500	0.002	0.0077	0.526	0.537	−3.18
5000	3.415	0.002	0.0077	0.596	0.435	2.98

TABLE IV. Parameters for the three cases studied; α_{TW} is the streamwise wavenumber of the traveling wave and $E_{u'}(t=0)$ is the initial energy of the fluctuations.

Re	α_{TW}	L_x	$E_{u'}$ $(t=0)$
3000	0.282	$2\pi/\alpha_{\mathrm{TW}}$	9.81×10^{-4}
3000	1.500	$4\pi/\alpha_{\mathrm{TW}}$	3.69×10^{-5}
5000	3.415	$8\pi/\alpha_{\mathrm{TW}}$	1.36×10^{-5}

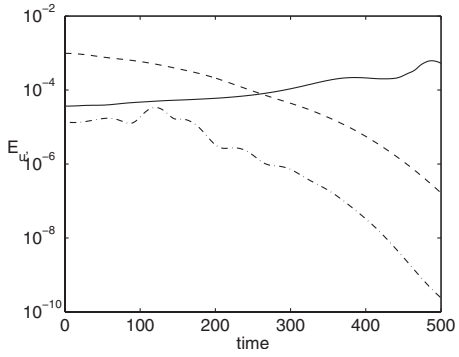

FIG. 11. Energy of the fluctuations vs time. We use as initial conditions the self-sustaining solutions represented by $\alpha_{TW}=0.282$ (dashed line) and $\alpha_{TW}=1.5$ (solid line) at Re=3000 and $\alpha_{TW}=3.415$ at Re=5000 (dash-dotted line).

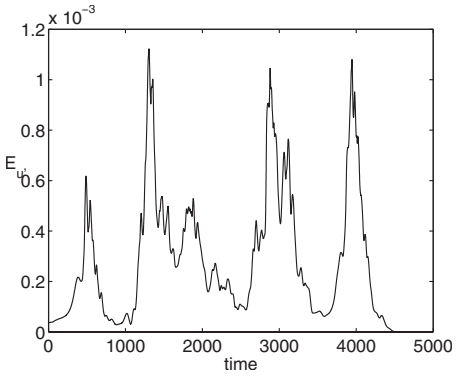

FIG. 13. Energy of the fluctuations vs time. We use as an initial condition the self-sustaining solution represented by $\alpha_{TW}=1.5$ at Re=3000.

times. Figure 12 shows the time variation in the energy of the mean flow, i.e., the laminar solution, plus the streaks, plus the rolls. By extracting the mean flow field at various instants one observes how the flow alternates in time from the evenly distributed four-vortex state obtained from the self-sustaining analysis to other topologies before reverting to the laminar state at approximately $t=5000$, where the energy of the fluctuations decreases abruptly (see Fig. 13). The initial secondary flow in Fig. 12 displays four vortices symmetric about the bisectors and is maintained until $t\approx 500$. After time $t\approx 1000$ the flow is in a state which appears to be intermittently turbulent, as shown in Fig. 13, with a mean skin friction value, averaged from $t=1000$ to $t=4500$, equal to 0.0424. The time development of the skin friction is shown in Fig. 14. The secondary patterns at $t=900$ and 2400 in Fig. 12 present two pairs of vortices in the cross section; they are close to the two vertical and horizontal walls, respectively, which can thus be defined as "active" since it is there that the turbulent wall cycle operates (according to recent observations by Uhlmann *et al.*[47]) These active walls contain low speed streaks situated on the bisector. Averaging over a turbulent period ($500\leq t\leq 4500$) yields a flow pattern with eight vortices (see Fig. 12), although this average solution does not display symmetry about the diagonals, as shown, for example, by Gavrilakis.[46] This observation can be explained by the initial condition (the four-vortex state) still dominating the dynamics; for different initial solutions the familiar diagonally symmetric eight-vortex pattern ensues for the same value of Re after averaging in time.[50] For a geometrical description of the transition process, we choose the phase subspace spanned by two observables: The bulk Reynolds number Re_b (based on the bulk velocity) and the energy of the streamwise-averaged flow E_U. Figure 15 shows the trajectories from the initial condition at $\mathrm{Re}_b=1032$, $E_U=0.0733$ to the laminar fixed point at $\mathrm{Re}_b=1431$, $E_U=0.1568$. The turbulent mean values are $\mathrm{Re}_b=976$, $E_U=0.0650$. For $\alpha_{TW}=1.5$ and Re=3000 (left figure) the trajectory orbits around the point which characterizes the fully developed turbulent state and, before the end of the last orbit, it escapes through the unstable manifold of the saddle point toward the laminar fixed point. For the other streamwise wavenumber $\alpha_{TW}=0.282$, we start at the same initial point in Fig. 15 and observe a monotonic decay back to the laminar fixed point. A similar pattern as for $\alpha_{TW}=0.282$ is observed for the initial condition with $\alpha_{TW}=3.415$ at Re=5000.

The flow dynamics that result from the initial conditions at $\alpha_{TW}=0.282$, Re=3000 and $\alpha_{TW}=3.415$, Re=5000 displays a direct escape of the flow back to the laminar flow without any cyclic or quasicyclic trajectory in phase space.

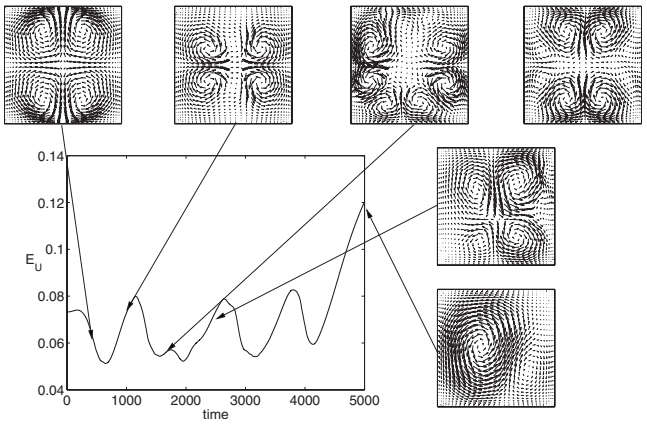

FIG. 12. The energy of the mean flow vs time. We use as an initial condition the self-sustaining solutions represented by $\alpha_{TW}=1.5$ at Re=3000. The time-averaged eight-vortex state is also shown (top right); it is not symmetric with respect to the diagonals of the cross section.

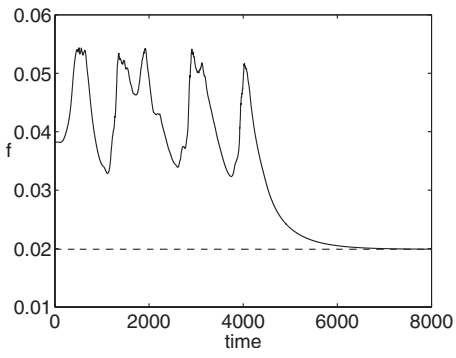

FIG. 14. The skin friction f vs time. We use as an initial condition the self-sustaining solution represented by $\alpha_{TW}=1.5$ at Re=3000. The mean skin friction value, averaged from $t=1000$ to $t=4500$, equals 0.0424. The skin friction for the laminar flow equals 0.02 (dashed line).

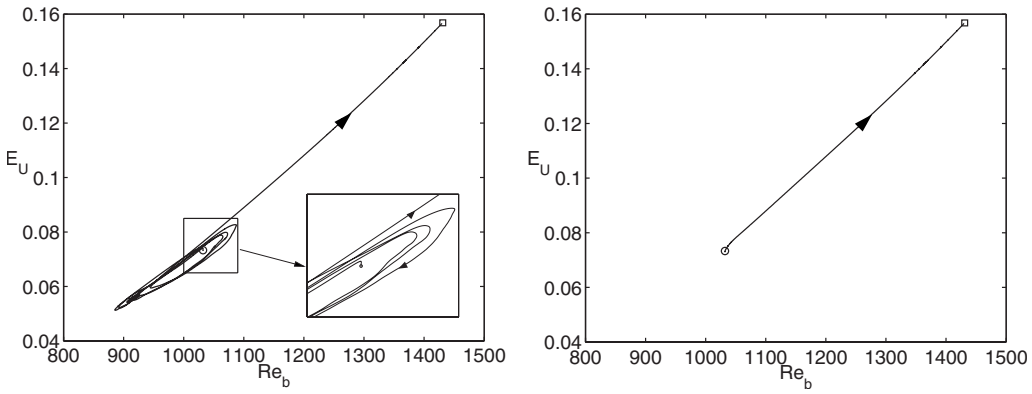

FIG. 15. The initial condition (circle) corresponds to the self-sustaining solution represented by $\alpha_{TW}=1.5$ (left figure) and $\alpha_{TW}=0.282$ (right figure) at Re $=3000$. Both initial conditions correspond to $\mathrm{Re}_b=1032$ and $E_U=0.0733$. The arrows indicate the direction in which the time increases. The ideal laminar flow corresponds to $\mathrm{Re}_b=1431$ (Re$=3000$) and $E_U=0.1568$ and is indicated by a square.

The traveling wave disappears and the flow relaxes to a streamwise independent state which slowly decays back to the laminar flow on a long viscous time scale. In contrast, the initial condition at $\alpha_{TW}=1.5$, Re$=3000$ results in a chaotic tangling of the time-dependent trajectories involving a large spectrum of time scales. Thus, at Re$=3000$, the flow presents two manifolds, one leading to the laminar state (associated here with $\alpha=0.282$) and the second toward the turbulent state and characterized by shorter waves.

Performing a parametric study over the Reynolds number, the SSP solutions would typically present an upper and a lower branch through a (saddle-node) bifurcation. Wang *et al.*[45] described the lower branch properties of the coherent solution in Couette flow. In a phase space spanned by the energy input and energy dissipation rate, the lower branch was shown to be situated in the intermediate area between the laminar and the turbulent attractors. The upper branch was found to be located within the chaotic orbits and capable of capturing the key statistics of the turbulent flow, see also Ref. 31. Wang *et al.*[45] suggested that the lower branch is on the separatrix between the basin of attraction of the laminar state and that of the turbulent state. Indeed, such a point is a saddle with low dimensional unstable manifolds (this point is shown in Fig. 15 with an empty circle), and it sits on the projection onto the chosen space of the separatrix between laminar flow and turbulence. Thus, to trigger transition, it is necessary to perturb the laminar state in such a way that the perturbed flow approaches the lower branch solution (along a stable manifold) and then let the flow evolve to the turbulent state (along the unstable manifold).

By comparing the two frames in Fig. 15 and considering an initial condition composed of the weighted sum of both traveling wave solutions, the statement that the circle of Fig. 15 sits on the laminar/turbulent separatrix can be better appreciated. A simulation with this initial condition is, however, not feasible because we need to find a common period (streamwise length) for these two traveling waves, which is very large in our case.

V. CLOSING REMARKS

Three approximate solutions to the Navier–Stokes equations have been discovered in a square duct using the SSP procedure proposed by Waleffe.[3] As initial conditions we used the least stable rolls solutions, corresponding to four vortices, and the second to least stable rolls (eight vortices) to produce streamwise streaks. However, using the eight-vortex state in the parametric study performed, we were not able to identify a SSP solution, which was found to correspond only to the four-vortex state. By locating appropriate neutrally stable waves, obtained from the stability analysis of the streaky flow, and then by their quadratic interaction to reproduce the initial rolls, approximate nonlinear self-sustaining states were discovered. Three approximate solutions have been found only for the least stable rolls for $\alpha=0.282$ and $\alpha=1.5$ at Re$=3000$ and for $\alpha=3.415$ at Re $=5000$ for a well-defined symmetry of the linear waves. These solutions have been used as initial conditions in direct numerical simulations, showing either a monotonic decay to the laminar duct flow ($\alpha=0.282$) or a sustainment for either short ($\alpha=3.415$) or long times ($\alpha=1.5$).

The SSP solution is a traveling wave formed by four vortices in the cross section, symmetric about the bisectors, and appears to be situated in a space contained within the turbulent orbits in the chosen phase space representation. Similar solutions have been very recently observed by Uhlmann *et al.*[47] and Biau *et al.*[50] A nonlinear continuation approach is under way to discover the nonlinear exact coherent states.

ACKNOWLEDGMENTS

The financial support of the EU (Program Marie Curie Grant No. EST FLUBIO 20228-2006) and of the Italian Ministry of University and Research (Grant No. PRIN 2005-092015-002) are gratefully acknowledged. H.W. wishes to acknowledge also the support from the Foundation Blanceflor Boncompagni-Ludovisi as well as the Japan Society for the Promotion of Science (JSPS).

[1]O. Reynolds, "An experimental investigation of the circumstances which determine whether the motion of water shall be direct or sinuous, and of the law of resistance in parallel channels," Philos. Trans. R. Soc. London **174**, 935 (1883).
[2]M. J. Lee, J. Kim, and P. Moin, "Structure of turbulence at high shear rates," J. Fluid Mech. **216**, 561 (1990).
[3]F. Waleffe, "On a self-sustaining process in shear flows," Phys. Fluids **9**, 883 (1997).
[4]G. Hagen, "Uber die bewegung des wassers in engen zylidrischen rohren," Ann. Phys. Chem. **46**, 423 (1839).
[5]J. Poiseuille, "Recherches expérimentales sur le mouvement des liquides dans les tubes de trés petits diamétres," Compt. Rend. **11**, 961 (1840); **12**, 112 (1841); **9**, 433 (1846).
[6]T. Sexl, "Zur stabilitatsfrage der Poiseuilleschen and Couetteschen stromung," Ann. Phys. **83**, 835 (1927).
[7]T. Sexl, "Uber dreidimensionale storungen der Poiseuilleschen stromung," Ann. Phys. **84**, 807 (1927).
[8]P. J. Schmid and D. S. Henningson, "Optimal energy density growth in Hagen-Poiseuille flow," J. Fluid Mech. **277**, 197 (1994).
[9]G. M. Corcos and J. R. Sellars, "On the stability of fully developed flow in a pipe," J. Fluid Mech. **5**, 97 (1959).
[10]A. Davey and P. G. Drazin, "The stability of Poiseuille flow in a pipe," J. Fluid Mech. **36**, 209 (1969).
[11]A. Meseguer and L. N. Trefethen, "Linearized pipe flow to Reynolds number 10^7," J. Comput. Phys. **186**, 178 (2003).
[12]A. G. Darbyshire and T. Mullin, "Transition to turbulence in constant-mass-flux pipe flow," J. Fluid Mech. **289**, 83 (1995).
[13]B. Hof, A. Juel, and T. Mullin, "Scaling of the turbulence transition threshold in a pipe," Phys. Rev. Lett. **91**, 244502 (2003).
[14]J. Peixinho and T. Mullin, "Decay of turbulence in pipe flow," Phys. Rev. Lett. **96**, 094501 (2006).
[15]J. Peixinho and T. Mullin, "Recent observations in the transition to turbulence in a pipe," in *Proceedings of the IUTAM Symposium on Laminar-Turbulent Transition*, edited by R. Govindarajan (Springer, Bangalore, 2006), p. 45.
[16]I. Gavarini, A. Bottaro, and F. T. M. Nieuwstadt, "The initial stage of transition in cylindrical pipe flow: Role of optimal base-flow distortions," J. Fluid Mech. **517**, 131 (2004).
[17]T. Tatsumi and T. Yoshimura, "Stability of the laminar flow in a rectangular duct," J. Fluid Mech. **212**, 437 (1990).
[18]V. Theofilis, P. W. Duck, and J. Owen, "Viscous linear stability analysis of rectangular duct and cavity flows," J. Fluid Mech. **505**, 249 (2004).
[19]M. Uhlmann and M. Nagata, "Linear stability of flow in an internally heated rectangular duct," J. Fluid Mech. **551**, 387 (2006).
[20]B. Galletti and A. Bottaro, "Large-scale secondary structures in duct flow," J. Fluid Mech. **512**, 85 (2004).
[21]A. Bottaro, H. Soueid, and B. Galletti, "Formation of secondary vortices in turbulent square-duct flow," AIAA J. **44**, 803 (2006).
[22]J. Jimenez, "Coherent structures and dynamical systems," in *Proceedings of the 1987 Summer Program of Center for Turbulence Research* (Stanford University, Stanford, CA, 1987), Paper No. SEE N88-23086 16-34, pp. 323–324.
[23]H. Wedin, "Nonlinear solutions to pipe flow," Ph.D. thesis, University of Bristol, 2004.
[24]H. Wedin and R. R. Kerswell, "Exact coherent structures in pipe flow: Travelling wave solutions," J. Fluid Mech. **508**, 333 (2004).
[25]R. R. Kerswell, "Recent progress in understanding the transition to turbulence in a pipe," Nonlinearity **18**, R17 (2005).
[26]H. Faisst and B. Eckhardt, "Travelling waves in pipe flow," Phys. Rev. Lett. **91**, 224502 (2003).
[27]B. Hof, C. W. H. van Doorne, J. Westerweel, F. T. M. Nieuwstadt, H. Faisst, B. Eckhardt, H. Wedin, R. R. Kerswell, and F. Waleffe, "Experimental observation of nonlinear traveling waves in turbulent pipe flow," Science **305**, 1594 (2004).
[28]B. Hof, C. W. H. van Doorne, J. Westerweel, and F. T. M. Nieuwstadt, "Turbulence regeneration in pipe flow at moderate Reynolds numbers," Phys. Rev. Lett. **95**, 214502 (2005).
[29]I. J. Wygnanski and F. H. Champagne, "On transition in a pipe. Part 1. The origin of puffs and slugs and the flow in a turbulent slug," J. Fluid Mech. **59**, 281 (1973).
[30]I. J. Wygnanski, M. Sokolov, and D. Friedman, "On transition in a pipe. Part 2. The equilibrium puff," J. Fluid Mech. **69**, 283 (1975).
[31]F. Waleffe, "Homotopy of exact structures in plane shear flows," Phys. Fluids **15**, 1517 (2003).
[32]G. Kawahara and S. Kida, "Periodic motion embedded in plane Couette turbulence: Regeneration cycle and burst," J. Fluid Mech. **449**, 291 (2001).
[33]R. R. Kerswell and O. R. Tutty, "Recurrence of travelling waves in transitional pipe flow," J. Fluid Mech. **584**, 69 (2007).
[34]H. Faisst and B. Eckhardt, "Sensitivity dependence on initial conditions in transition to turbulence in pipe flow," J. Fluid Mech. **504**, 343 (2004).
[35]A. P. Willis and R. R. Kerswell, "Critical behaviour in the relaminarization of localized turbulence in pipe flow," Phys. Rev. Lett. **98**, 014501 (2007).
[36]B. Hof, J. Westerweel, T. M. Schneider, and B. Eckhardt, "Finite lifetime of turbulence in shear flows," Nature (London) **443**, 59 (2006).
[37]B. Eckhardt, T. M. Schneider, B. Hof, and J. Westerweel, "Turbulence transition in pipe flow," Annu. Rev. Fluid Mech. **39**, 447 (2007).
[38]M. Nagata, "Three-dimensional finite amplitude solutions in plane Couette flow: Bifurcation from infinity," J. Fluid Mech. **217**, 519 (1990).
[39]N. Tillmark and H. Alfredsson, "Experiments on transition in plane Couette flow," J. Fluid Mech. **235**, 89 (1992).
[40]S. Bottin, O. Dauchot, F. Daviaud, and P. Manneville, "Experimental evidence of streamwise vortices as finite amplitude solutions in transitional plane Couette flow," Phys. Fluids **10**, 2597 (1998).
[41]O. Dauchot and F. Daviaud, "Finite amplitude perturbation and spots growth mechanism in plane Couette flow," Phys. Fluids **7**, 335 (1995).
[42]A. Lundbladh and A. V. Johansson, "Direct simulation of turbulent spots in plane Couette flow," J. Fluid Mech. **229**, 499 (1991).
[43]D. Viswanath, "Recurrent motions within plane Couette turbulence," J. Fluid Mech. **580**, 339 (2007).
[44]C. Pringle and R. R. Kerswell, "Asymmetric, helical and mirror-symmetric travelling waves in pipe flow," Phys. Rev. Lett. **99**, 074502 (2007).
[45]J. Wang, J. Gibson, and F. Waleffe, "Lower branch coherent states in shear flows: Transition and control," Phys. Rev. Lett. **98**, 204501 (2007).
[46]S. Gavrilakis, "Numerical simulation of low-Reynolds-number turbulent flow through a straight square duct," J. Fluid Mech. **244**, 101 (1992).
[47]M. Uhlmann, A. Pinelli, G. Kawahara, and A. Sekimoto, "Marginally turbulent flow in a square duct," J. Fluid Mech. **588**, 153 (2007).
[48]A. Huser and S. Biringen, "Direct numerical simulation of turbulent flow in a square duct," J. Fluid Mech. **257**, 65 (1993).
[49]F. B. Gessner, "The origin of secondary flow in turbulent flow along a corner," J. Fluid Mech. **58**, 1 (1973).
[50]D. Biau, H. Soueid, and A. Bottaro, "Transition to turbulence in duct flow," J. Fluid Mech. **596**, 133 (2008).
[51]F. Waleffe, "Three-dimensional coherent states in plane shear flows," Phys. Rev. Lett. **81**, 4140 (1998).
[52]S. J. Kline, W. C. Reynolds, F. A. Schraub, and P. W. Runstadler, "The structure of turbulent boundary layers," J. Fluid Mech. **30**, 741 (1967).